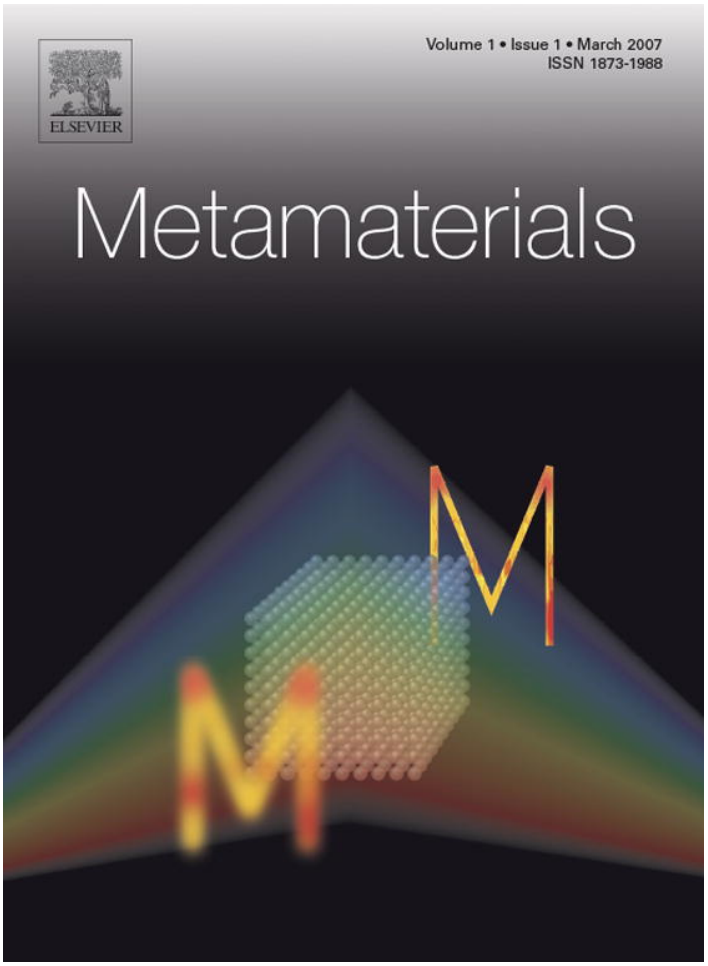

Available online at www.sciencedirect.com
ScienceDirect
Metamaterials 1 (2007) 44–51
Metamaterials
www.elsevier.com/locate/metmat

Higher order interactions in magneto-inductive waveguides

R.R.A. Syms [a,*], O. Sydoruk [b], E. Shamonina [b], L. Solymar [a]

[a] *Optical and Semiconductor Devices Group, EEE Department, Imperial College, Exhibition Road, London SW7 2AZ, UK*
[b] *Department of Physics, University of Osnabruck, 49060 Osnabruck, Germany*

Received 20 December 2006; received in revised form 30 January 2007; accepted 2 February 2007
Available online 12 February 2007

Abstract

The properties of periodic chains of magnetically coupled L–C resonators supporting magneto-inductive (MI) waves are examined in the case when non-nearest neighbour interactions are significant. The variation of the coupling coefficient with separation is measured using resonant elements based on printed circuit board inductors and surface mount capacitors, and used to predict the S-parameters and dispersion characteristics of magnetoinductive waveguides. Good agreement with experimental measurements is obtained when higher order interactions are included. The significance of non-nearest neighbour interactions in more general MI wave devices is then highlighted in an example problem involving reflection from a waveguide discontinuity, and the influence of higher order evanescent waves is discussed.

PACS: 41.20.Jb

Keywords: Electromagnetic theory; Waveguide; Magneto-inductive wave; Metamaterial

1. Introduction

A magnetoinductive (MI) wave is a form of slow-wave that may propagate on a system of coupled L–C resonators. Both forward and backward waves may be supported, depending on the arrangement of the resonators (and hence on the sign of the magnetic coupling). MI waves were mentioned in textbooks in the 1960s and 1970s in connection with periodic filters [1] and slow wave structures [2,3], and similar waves have been exploited more recently in planar slow wave filters [4]. They were recently resurrected by Shamonina et al. [5] in the context of metamaterials, and experimental confirmation for a set of capacitively loaded loops was provided by Wiltshire et al. [6]. The initial analysis for a one-dimensional MI waveguide was generalised to two and three dimensions [7], and laws of reflection and refraction have been developed for MI waves that are analogous to Snell's law for electromagnetic (EM) waves [8]. Specifically designed resonant elements with attenuation as small as 0.12 dB per element have been recently described [9]. MI waveguides are a variant of the wider subject of metamaterials, which have been of considerable interest recently [10–14].

Applications for MI waves are now emerging, since their slow speed has the potential to allow the processing of low frequency signals in a compact structure. Planar MI waveguide transducers have been developed [15], and phase shifters have been investigated [16]. Imaging has been demonstrated using parallel two-dimensional sheets of coupled resonators [17,18]. One-dimensional

* Corresponding author. Tel.: +44 207 594 6203; fax: +44 207 594 6308.
E-mail address: r.syms@imperial.ac.uk (R.R.A. Syms).

1873-1988/$ – see front matter © 2007 Published by Elsevier B.V.
doi:10.1016/j.metmat.2007.02.005

waveguide devices have received considerable attention, and tapered concentrators [19], mirrors, interferometers, splitters, Bragg gratings and couplers have all been investigated [20].

Most of the analysis of MI waves to date has been based on lumped element models similar to the mechanical models developed many years ago for crystals [21] and more recently for other metamaterials with magnetic coupling between nearest-neighbour elements [22,23]. The generalisation to higher order interactions is quite straightforward [7]. The need to take into account a number of higher order interactions had already arisen when matching theory to experiment, for example, using the so-called 'Swiss Roll' resonators [24]. Also, in a theoretical paper concerned with retardation effects, all interactions in a hundred-element array had to be considered [25]. However, there has been no analysis so far of the effect of higher order interactions either on the dispersion equation itself or on the operational characteristics of MI wave devices.

The aim of the present paper is therefore to investigate the effect of higher-order interactions in magneto-inductive waveguides in more detail. Section 2 provides a brief overview of the theoretical formulation of the dispersion equation for higher-order interactions. Experimental measurements of the coupling coefficients between pairs of resonant elements, and the scattering parameters and dispersion characteristics of waveguides are presented in Section 3, and a comparison between theory and experiment is made in Section 4. The theory including second order interaction is applied to a simple MI waveguide device – a reflector – in Section 5. Conclusions are drawn in Section 6.

2. Theoretical dispersion characteristic

We shall consider a one-dimensional array of magnetically coupled resonant elements, shown schematically in Fig. 1a as a set of capacitively loaded loops arranged in the so-called "axial configuration" with a regular separation d. The array is assumed to be infinitely long, and each element is coupled magnetically to every other element. The elements are modeled as resonant circuits consisting of an inductor L, a capacitor C and a resistor R. Note that the length of the array is assumed to be small relative to the free space wavelength so that retardation effects may be neglected. Using Kirchoff's voltage law, the dispersion equation may be obtained in the form [7]:

$$\left\{1 - \frac{\omega_0^2}{\omega^2} - \frac{j}{Q}\right\} + \sum_{\nu=1}^{N} \kappa_\nu \cos(\nu k d) = 0 \qquad (1)$$

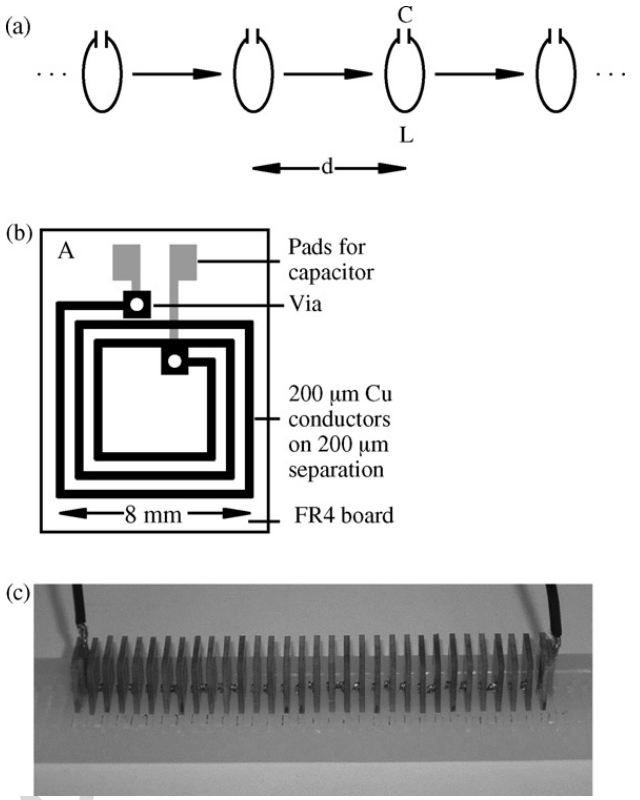

Fig. 1. (a) Schematic of a magnetoinductive waveguide; (b) PCB layout of resonant element, and (c) experimental arrangement of a magneto-inductive waveguide.

Here ω is the angular frequency, $\omega_0 = (LC)^{-1/2}$ is the corresponding resonant frequency and $Q = \omega_0 L/R$ is the quality factor. For νth nearest neighbours, $\kappa_\nu = 2M_\nu/L$ is the coupling coefficient and M_ν is the mutual inductance. The propagation constant is $k = \beta - j\alpha$, where βd and αd describe the phase shift and attenuation per element, respectively. In the case when losses are low and only nearest neighbour coupling is significant, Eq. (1) has a single propagating wave solution, which exists over the frequency band $1/(1+\kappa_1) \leq (\omega/\omega_0)^2 \leq 1/(1-\kappa_1)$. More generally, for real values of k and ω, Eq. (1) leads in most cases to a monotonically increasing dispersion curve (see Section 5 for an exception). However, additional solutions can now be found, considering that $\cos(\nu kd)$ can be expanded into νth order Chebyshev polynomials of $\cos(kd)$. In those solutions, k may turn out to be either complex or purely imaginary. Usually, these solutions are of no practical significance, but they will be needed in the presence of discontinuities in the waveguide. We shall return to this problem in Section 5.

3. Experimental results

MI waveguides were constructed to investigate their dispersion characteristic and find their properties in

reflection and transmission, using an Agilent E5061A Network Analyser for electrical measurements. The experiments were performed on planar three-turn inductors formed on FR-4 substrates as shown in Fig. 1b and made resonant using additional surface mount capacitors. The inductance and capacitance were $L = 140$ nH and $C = 100$ pF, respectively, giving a resonant frequency of $f_0 \approx 42$ MHz. These values were obtained using a needle probe for excitation; similar resonant frequencies were obtained using a weakly coupled exciting coil. At this frequency, the Q-factor (found from measurements of bandpass characteristics) was 50. The resonances of individual elements were matched to ± 0.1 MHz, and magneto-inductive waveguides were constructed by inserting resonant elements into a plastic baseboard carrying an array of regularly spaced slots. The baseboards were formed using a numerically controlled machine tool, with a tolerance of ± 25 μm. A 30-element line is shown in Fig. 1c.

Input and output coupling was carried out by connecting 50 Ω transmission lines from the network analyzer to additional planar two-turn inductors with an inductance $L_T \approx 78$ nH, which were then inductively coupled to the first and last element in the array. This method has previously been shown to give good broad band matching between a transmission line and a MI waveguide, provided the matching elements are suitably chosen [9].

The properties of the waveguide depend crucially on the coupling coefficient between the elements. κ was determined from the resonances of a two-element system, which was probed with a weakly coupled coil as shown in Fig. 2a and described in more detail in [9]. This method yields the resonant frequencies of a system that depends only on nearest neighbour coupling, as $\omega^2 = 1/\{(L \pm M_1)C\} = \omega_0^2/(1 \pm M_1/L)$, allowing the value of M_1/L (and hence κ_1) to be determined. The values of the measured coupling coefficient are plotted in Fig. 2b as a function of the axial separation d. It is worth noting that the theoretical maximum value of κ_1 is 2, and this is the first time that coupling coefficients as high as 1.6 have been found.

We have been unable to match the measured coupling coefficients with the simple analytical theory based on circular single-turn coils, since the field is quite different between two of our closely spaced multi-turn coils. However, we have found that the inverse polynomial

$$\kappa(d) = \{a_0 + a_1 d + a_2 d^2 + a_3 d^3 + a_4 d^4 + a_5 d^5\}^{-1} \qquad (2)$$

has suitable asymptotic properties and matches the experimental results very well for the parameter values $a_0 = 5.5e^{-1}$, $a_1 = 5.7e^{-1}$, $a_2 = -2.0e^{-2}$, $a_3 = 3.7e^{-2}$, $a_4 = -3.8e^{-3}$ and $a_5 = 1.9e^{-4}$, as shown by the line in Fig. 2b. The experiments were repeated using elements resonant at 133 MHz, and similar agreement was obtained.

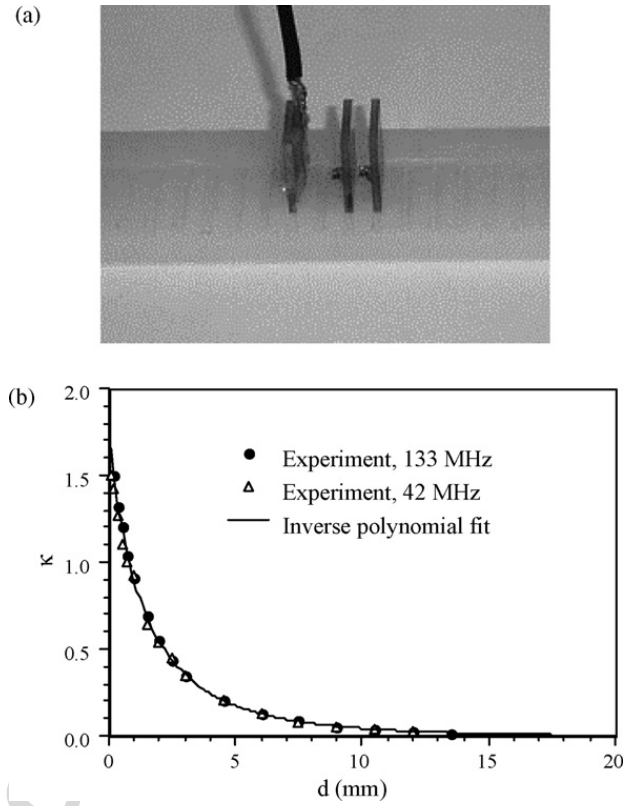

Fig. 2. (a) Experimental arrangement for determination of the coupling coefficient; (b) variation of coupling coefficient κ with axial element separation d.

Transmission and reflection measurements were made on the 30-element line shown in Fig. 1c, for an axial separation of $d = 3.5$ mm, yielding the scattering coefficients S_{11} and S_{12}. The frequency variation of their modulus is plotted as the bold lines in Fig. 3a and b, respectively. Transmission is obtained over a narrow frequency band, ranging from ≈35 to ≈48 MHz. The maximum transmission occurs at a frequency of ≈40 MHz, and (ignoring coupling losses) corresponds to a propagation loss of ≈0.5 dB per element. The minimum reflection occurs at the slightly higher frequency of 45 MHz.

The dispersion characteristics were determined by measuring the phase delay arg(S_{12}) and dividing by the number of elements in the line to yield the dispersion characteristic shown by the bold line in Fig. 4. As predicted, low-loss propagation is obtained only over a narrow frequency band, but propagation with increasing loss may still be obtained outside the band edges.

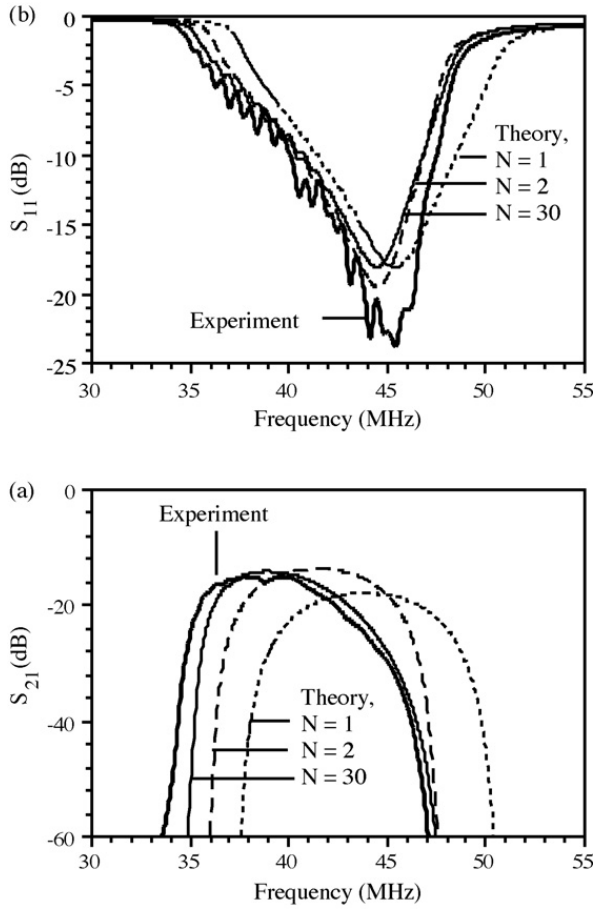

Fig. 3. Frequency variation of (a) $|S_{11}|$ and (b) $|S_{21}|$ for a 30-element MI waveguide with 3.5 mm axial element separation. Bold lines show experimental data, and ordinary lines show theoretical predictions obtained using the measured coupling coefficient variation including interactions up to $N = 1$, 2 and 30.

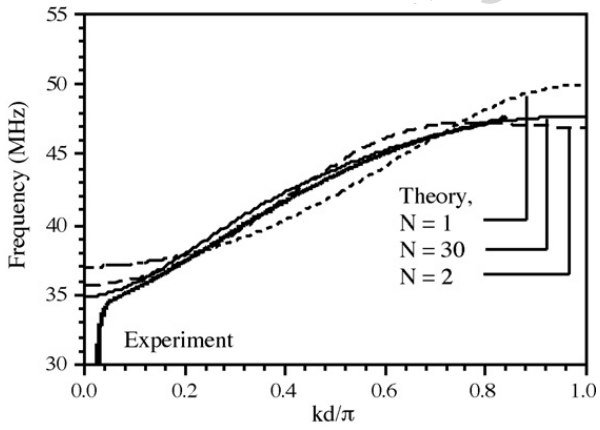

Fig. 4. Dispersion characteristic of a 30-element MI waveguide with 3.5 mm axial element separation. Bold lines show experimental data and ordinary lines show theoretical predictions obtained using the measured coupling coefficient variation including interactions up to $N = 1$, 2 and 30.

4. Comparison between theory and experiment

Transmission through the MI waveguide system was modelled by constructing the impedance matrix, and using the standard definition of the scattering parameters in terms of the currents and voltages at the input and output [26] to obtain their values as a function of frequency. For the MI waveguide itself, the circuit elements L, R and M_ν were obtained from the experimental data previously described. At the experimental spacing, the nearest neighbour coupling coefficient was $\kappa_1 \approx 0.29$. For the input and output transducers, the element inductance L_T was as previously given, while the mutual inductance M_T describing coupling to the line was estimated as $M_T = \eta (LL_T)^{0.5}$, where η is a constant such that $0 \leq \eta \leq 1$ [27]. In the event, a best-fit value was obtained as $\eta \approx 0.55$.

The thin lines in Fig. 3a and b show theoretical results for S_{11} and S_{21} respectively. Three cases have been considered, namely when (i) nearest neighbour, (ii) next nearest neighbour, and (iii) all interactions are taken into account. For S_{21}, it may be clearly seen that the theoretical curve closest to the experimental data is for all interactions. Given that the calculations are somewhat involved in this case, an interesting question is, how many interactions should be included to get reasonable agreement in a model with only moderate complexity? Further investigation showed that five interactions are sufficient. The situation is somewhat different for S_{11}. With $Q = 50$, the waveguide is so lossy that non-neighbouring elements are likely to have less influence on reflection than on transmission. Hence, there is little difference between the theoretical results for different number of interactions.

Theoretical dispersion curves can be calculated from Eq. (1), considering only the low attenuation solution. The thin lines in Fig. 4 show the results for the same cases (i)–(iii). Clearly, there is again improved agreement between theory and experiment as high order interactions are included.

5. MI waveguide devices

The introduction of non-nearest neighbour coupling may have significant consequences for magnetoinductive waveguide devices. To see the likely effects, we consider the typical, and relatively simple, problem of the discontinuity that may arise when one of the elements in an otherwise uniform waveguide is placed at a different distance from its neighbour as shown in Fig. 5a. The discontinuity will act as mirror, and its properties have already been estimated using nearest neighbour theory [20].

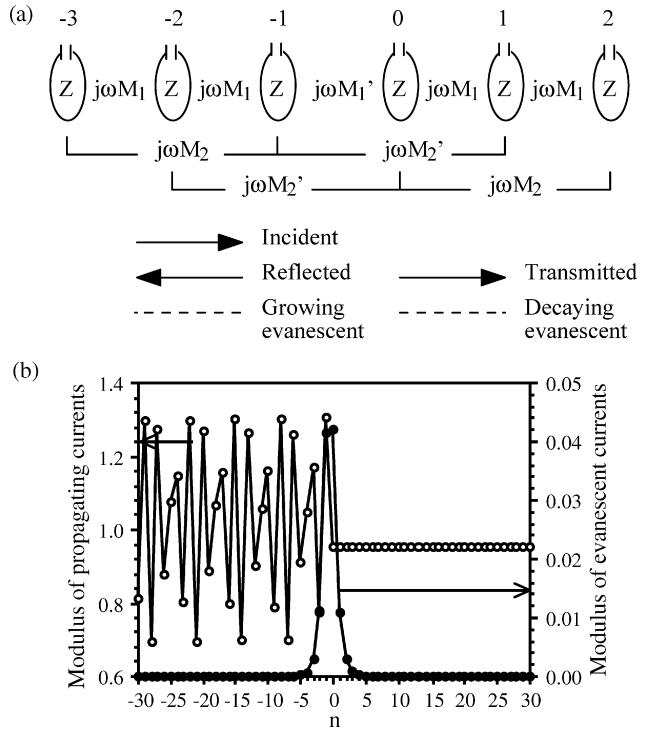

Fig. 5. (a) MI waveguide mirror formed by a local variation in the element spacing d, (b) local variations of the currents near an interface, for $\kappa_1 = 0.2$, and $\mu = 0.7$, assuming a quadratic decay in coupling coefficient and a second nearest neighbour model.

The aim is here to find a more accurate solution, by allowing coupling up to Nth order. The question again arises how large should N be. In nearest neighbour theory, the boundary-matching problem at the interface can be described using two equations, corresponding to the two unknowns (the transmitted and reflected wave amplitudes). If Nth order interactions are considered, there will be $2N$ unknowns, one for the amplitude of each solution, resulting in a considerable increase in calculation effort. Furthermore, the dispersion equation must be solved to find the complex propagation constants of a set of N waves. In this case, we have found that if second-nearest neighbour interactions are included, a simple analytic solution may still be obtained for both the dispersion equation and the boundary problem.

Considering first the dispersion equation, we see that for $N = 2$, Eq. (1) may be written as a quadratic in $\cos(kd)$. In the lossless case, we obtain:

$$\left\{1 - \frac{\omega_0^2}{\omega^2}\right\} + \kappa_1\{\cos(kd) + \zeta[2\cos^2(kd) - 1]\} = 0 \quad (3)$$

Here $\zeta = \kappa_2/\kappa_1$ is the ratio of the second-nearest and nearest coupling coefficients. Eq. (3) is a quadratic in $\cos(kd)$, and hence may be solved exactly using the standard method. For small ζ, analytic approximations may also be obtained for the roots. The following results are obtained. For small ζ, ω increases monotonically with kd. In this case, there is only one propagating wave solution. However, for higher values of ζ, the ω-k diagram has a subsidiary maximum between $kd = 0$ and $kd = \pi$ and a second propagating wave appears. It is simple to show by differentiation that the subsidiary maximum first appears when $\zeta = 0.25$. In this case the dispersion curve is very similar to that shown in Fig. 4, for $N = 2$, with a relatively flat plateau between $kd/\pi = 0.8$ and $kd/\pi = 1.0$, and is therefore a reasonably realistic representation of the experimental situation here.

Because the case of a non-monotonic dispersion characteristic is somewhat unrealistic, we consider only the situation when $\zeta \leq 0.25$. In this case, the propagation constants for both waves may be found by solving Eq. (3) using the standard analytic method for a quadratic equation. The primary solution has a real value of kd and corresponds to a propagating magneto-inductive wave. The secondary solution has the complex value $kd = \pi \pm j\alpha d$, and is therefore an evanescent wave, whose modulus decays exponentially and whose sign alternates between adjacent elements.

Considering now the interface problem, we can see in Fig. 5a that the uniformity of the waveguide is perturbed by having a separation between elements -1 and 0 that is different from the rest. The mutual impedance between this pair of elements is $j\omega M_1'$ while the mutual impedances between any other two neighbouring elements is $j\omega M_1$. The new feature not considered in [20] is the mutual impedance between second nearest neighbours, which is $j\omega M_2$ in the uniform part of the waveguide, and $j\omega M_2'$ between elements -2 and 0 and between elements -1 and 1.

Clearly, the terms M_1, M_1', M_2 and M_2' may in general be found from a coupling coefficient variation of the type already shown in Fig. 2b. In the calculations that follow, we have assumed a simpler power law:

$$\kappa(d) = bd^{-2} \quad (4)$$

This variation is representative of mid-range values of κ in Fig. 2b, and allows analytic expressions for parameter values to be obtained. Thus, for example, it is simple to show that $\zeta = M_2/M_1 = 0.25$, and other similar ratios may be derived easily.

The governing equations near the interface may be obtained by writing Kirchhoff's voltage law for elements -2, -1, 0 and 1 as:

$$ZI_{-2} + j\omega M_1\{I_{-1} + I_{-3}\} + j\omega M_1' I_0 + j\omega M_2 I_{-4} = 0$$

$$ZI_{-1} + j\omega M_1' I_0 + j\omega M_1 I_{-2} + j\omega M_2' I_1 + j\omega M_2 I_{-3} = 0$$

$$
\begin{aligned}
&ZI_0 + j\omega M_1 I_1 + j\omega M_1' I_{-1} \\
&\quad + j\omega M_2' I_{-2} + j\omega M_2 I_2 = 0 \\
&ZI_1 + j\omega M_1\{I_2 + I_0\} + j\omega M_2 I_3 + j\omega M_2' I_{-1} = 0
\end{aligned}
\tag{5}
$$

Here I_n is the current in the nth element and $Z = j\omega L + 1/j\omega C$ is the self-impedance of each element. To solve these equations, it is no longer possible to assume a single reflected wave and a single transmitted wave. We need two more waves, which, as mentioned earlier in this Section, are evanescent. In the present context it means that there will be two more waves falling off exponentially from the discontinuity, which we assume will have amplitudes A and B at the discontinuity itself. Thus we write:

$$
\begin{aligned}
I_n &= I_{00}\{\exp(-jnkd) + \Gamma\exp(+jnkd) + A\exp(-jn\pi)\exp(\alpha nd)\} \quad \text{for } n < 0 \\
I_n &= I_{00}\{T\exp(-jnkd) + B\exp(-jn\pi)\exp(-\alpha nd)\} \quad \text{for } n > -1
\end{aligned}
\tag{6}
$$

Here I_{00} is a constant and Γ and T are the amplitudes of the reflected and transmitted waves. Eq. (5) must be solved for the four unknowns Γ, T, A and B. Substituting Eq. (6) into Eq. (5) and using the dispersion equation, we obtain:

$$
\begin{aligned}
&-\zeta\Gamma + \xi T - \zeta A + \xi B = \zeta \\
&-\{1 + \zeta\exp(jkd)\}\Gamma + \{\mu + \xi\exp(-jkd)\}T \\
&-\{1 - \zeta\exp(\alpha d)\}A + \{\mu - \xi\exp(-\alpha d)\}B = \{1 + \zeta\exp(-jkd)\} \\
&-\{\mu\exp(-jkd) + \xi\exp(-j2kd)\}\Gamma + \{\exp(jkd) + \zeta\exp(j2kd)\}T \\
&+\{\mu\exp(-\alpha d) - \xi\exp(-2\alpha d)\}A - \{\exp(\alpha d) - \zeta\exp(2\alpha d)\}B = \{\mu\exp(jkd) + \xi\exp(j2kd)\} \\
&-\xi\exp(-jkd)R + \zeta\exp(jkd)T + \xi\exp(-\alpha d)A - \zeta\exp(\alpha d)B = \xi\exp(jkd)
\end{aligned}
\tag{7}
$$

Here we have introduced the further normalized quantities $\mu = M_1'/M_1$ and $\xi = M_2'/M_1$. Once μ has been defined, the value of ξ follows automatically from Eq. (4). Eq. (7) now represents the four required simultaneous equations. Before proceeding, we note that in the limit when ζ and $\xi \to 0$, A and B are negligible, so we obtain:

$$
\begin{aligned}
&1 + \Gamma = \mu T \\
&\mu\{\exp(jkd) + \exp(-jkd)\Gamma\} = \exp(jkd)T
\end{aligned}
\tag{8}
$$

Eq. (8) are identical to the corresponding equations obtained previously by neglecting second-nearest neighbour interactions [20].

Fig. 5b shows the local variation of current near the interface, found by solving Eq. (7) numerically by diagonalisation and back-substitution for the particular case of $\kappa_1 = 0.2$, $\mu = 0.7$, $\zeta = 0.25$ and $\omega/\omega_0 = 1$. Two plots are shown. The light circles show the variation of the modulus of the incident and reflected current on the left-hand side of the interface and the transmitted current on the right hand side; the dark circles show similar results for the evanescent currents. The incident and reflected currents form a standing wave pattern on the left-hand of the interface. The evanescent currents clearly have much smaller amplitudes, and decay rapidly on either side of the interface. Their decay rate depends on the value of αd, which may vary significantly depending on the value of ζ and ω/ω_0.

Fig. 6a shows the frequency variation of $|\Gamma|^2$ and $|T|^2$, again for $\kappa_1 = 0.2$, $\zeta = 0.25$ and $\mu = 0.7$. Two sets of data are shown. The thick lines show results obtained for nearest-neighbour interactions only, whereas the thin lines are calculated by including second order interactions as well. The results are qualitatively similar, but there is a shift of the characteristic to lower frequencies. Numerically, we have verified that the second neighbour model conserves power between the propagating waves so that $|\Gamma|^2 + |T|^2 = 1$ to a high degree of accuracy.

Fig. 6b shows the variation of $|\Gamma|^2$ and $|T|^2$ with μ, now assuming that $\omega = \omega_0$. Again, thick lines show the results for the nearest-neighbour model, while thin lines show the results including second-nearest neighbours as well. Once again, there are some differences between the curves indicating that for more accurate design work the nearest neighbour assumption is no longer tenable. Note that there is no difference between the two solutions when $\mu = 1$, since the discontinuity then vanishes.

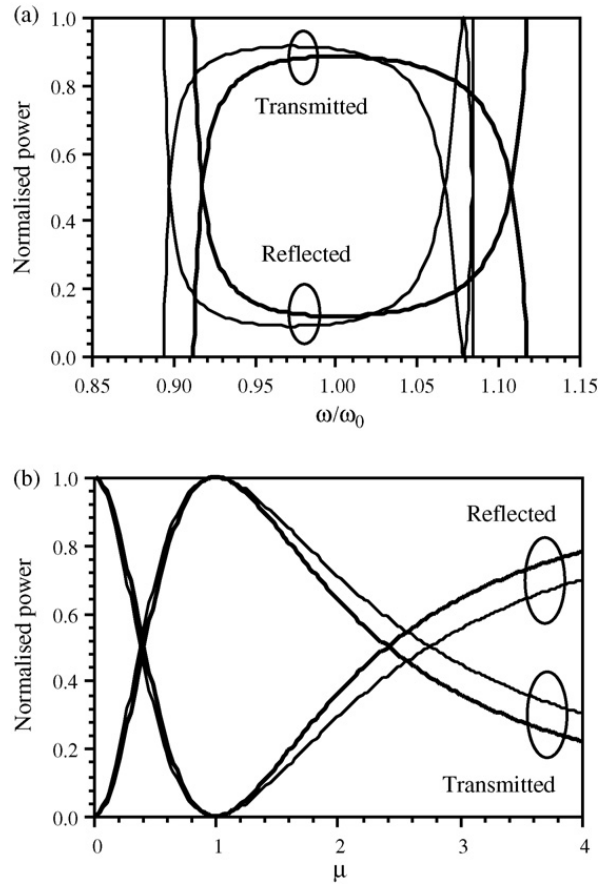

Fig. 6. (a) Variation of $|\Gamma|^2$ and $|T|^2$ with ω, in a waveguide mirror formed by a local variation in the element spacing d, assuming that $\kappa_1 = 0.2$ and $\mu = 0.7$, and that there is a quadratic decay in coupling coefficient; (b) corresponding variation with μ, assuming that $\kappa_1 = 0.2$ and $\omega = \omega_0$. Thick lines – nearest neighbour model; thin lines – second nearest neighbour model.

6. Conclusions

We have shown that higher-order interactions may not, in general, be neglected in magneto-inductive waveguides consisting of axially coupled planar resonant elements. However, their effects may be incorporated in the theory relatively simply, and accurate predictions of the performance of MI waveguides are obtained from models using a relatively small number of additional terms. More importantly, higher-order interactions have been shown to give rise to additional wave solutions at discontinuities, which significantly alter the performance characteristics of MI wave devices compared with the predictions of simple theory. There is therefore a strong incentive to develop element designs that suppress non-nearest neighbour interactions, for example using solenoidal inductors rather than planar elements.

Acknowledgements

This effort was sponsored by the Air Force Office of Scientific Research, Air Force Material Command, USAF, under grant number FA8655-1-3007. The U.S. Government is authorized to reproduce and distribute reprints for Governmental purpose, notwithstanding any copyright notation thereon. Two of us (E.S. and O.S.) also wish to thank the German Research Council for support.

References

[1] G. Atabekov, Linear Network Theory, Pergamon Press, Oxford, 1965.
[2] R.A. Silin, V.P. Sazonov, Slow wave structures, Boston SPA Eng. National Lending Library for Science and Technology (1971).
[3] C.C. Lee, L.C. Shen, Travelling waves in coupled Yagi structures, IEEE Trans. Microw. Theory Tech. 25 (1977) 931–933.
[4] J.S. Hong, M.J. Lancaster, Theory and experiment of novel microstrip slow-wave open-loop resonator filters, IEEE Trans. Microw. Theory Tech. 45 (1997) 2358–2365.
[5] E. Shamonina, V.A. Kalinin, K.H. Ringhofer, L. Solymar, Magneto-inductive waveguide, Electron. Lett. 38 (2002) 371–373.
[6] M.C.K. Wiltshire, E. Shamonina, I.R. Young, L. Solymar, Dispersion characteristics of magneto-inductive waves: comparison between theory and experiment, Electron. Lett. 39 (2003) 215–217.
[7] E. Shamonina, V.A. Kalinin, K.H. Ringhofer, L. Solymar, Magnetoinductive waves in one, two, and three dimensions, J. Appl. Phys. 92 (2002) 6252–6261.
[8] R.R.A. Syms, E. Shamonina, L. Solymar, Positive and negative refraction of magnetoinductive waves in two dimensions, Eur. Phys. J. B 46 (2005) 301–308.
[9] R.R.A. Syms, I.R. Young, L. Solymar, Low-loss magneto-inductive waveguides, J. Phys. D. Appl. Phys. 39 (2006) 3945–3951.
[10] J.B. Pendry, Negative refraction makes a perfect lens, Phys. Rev. Lett. 85 (2000) 3966–3969.
[11] J.B. Pendry, A.J. Holden, A.J. Robbins, W.J. Stewart, Magnetism from conductors and enhanced nonlinear phenomena, IEEE Trans. MTT 47 (1999) 2075–2084.
[12] D.R. Smith, W.J. Padilla, D.C. Vier, S.C. Nemat-Nasser, S. Schultz, Composite medium with simultaneously negative permeability and permittivity, Phys. Rev. Lett. 84 (2000) 4184–4187.
[13] R.A. Shelby, D.R. Smith, S. Schultz, Experimental verification of a negative index of refraction, Science 292 (2001) 77–79.
[14] D.R. Smith, J.B. Pendry, M.C.K. Wiltshire, Metamaterials and negative refractive index, Science 305 (2004) 788–792.
[15] M.J. Freire, R. Marques, F. Medina, M.A.G. Laso, F. Martin, Planar magneto-inductive wave transducers: theory and applications, Appl. Phys. Lett. 85 (2004) 4439–4441.
[16] I.S. Nefedov, S.A. Tretyakov, On potential applications of metamaterials for the design of broadband phase shifters, Microw. Opt. Tech. Lett. 145 (2005) 98–102.

[17] M.J. Freire, R. Marques, A planar magneto-inductive lens for 3D subwavelength imaging, Appl. Phys. Lett. 86 (2005) 182505-1-3.
[18] R. Marques, F. Mesa, M.J. Freire, J.D. Baena, Three-dimensional superresolution in metamaterial slab lenses: experiment and theory, Phys. Rev. B72 (2005) 235117.
[19] M.C.K. Wiltshire, E. Shamonina, I.R. Young, L. Solymar, Resonant magnetic concentrator, in: PIERS 2003 Symposium, October 13–16, Honolulu, Hawaii, USA, 2003.
[20] R.R.A. Syms, E. Shamonina, Solymar L, Magneto-inductive waveguide devices, IEE Proc. Microw. Antennas Propag. 153 (2006) 111–121.
[21] L. Brillouin, Wave propagation in periodic structures, McGraw-Hill Book Co. Ltd., New York, 1946.
[22] M. Rahman, M.A. Stuchly, Transmission line-periodic circuit representation of planar microwave photonic bandgap structures, Microw. Opt. Tech. Lett. 30 (2001) 15–19.
[23] G.V. Eleftheriades, A.K. Iyer, P.C. Kremer, Planar negative refractive index media using periodically L–C loaded transmission lines, IEEE Trans. Microw. Theory Tech. 50 (2002) 2702–2712.
[24] M.C.K. Wiltshire, E. Shamonina, I.R. Young, L. Solymar, Experimental and theoretical study of magneto-inductive waves supported by one-dimensional arrays of “swiss rolls”, J. Appl. Phys. 95 (2004) 4488–4493.
[25] O. Zhuromskyy, E. Shamonina, L. Solymar, Effect of radiation on dispersion of magneto-inductive waves in a metamaterial, Proc. SPIE 5955 (2005) 06-1-06-8.
[26] S. Ramo, J.R. Whinnery, T. Van Duzer, Fields and Waves in Communication Electronics, second ed., John Wiley and Sons, 1984.
[27] L. Solymar, Lectures on Electromagnetic Theory: A Short Course for Engineers, Oxford University Press, 1976.